A NUCLEATION THEORY OF CELL SURFACE CAPPING

Evangelos A. Coutsias†, Michael J. Wester†, Alan S. Perelson‡

† Department of Mathematics and Statistics
University of New Mexico
Albuquerque, NM 87131, USA

‡ Theoretical Biology and Biophysics
Los Alamos National Laboratory
Los Alamos, NM 87545, USA

Keywords: aggregation, phase-transition, addition reactions, capping, sol-gel transformation, nucleation

Abstract

We propose a new theory of cell surface capping based on the principles of nucleation. When antibody interacts with cell surface molecules, the molecules initially form small aggregates called patches that later coalesce into a large aggregate called a cap. While a cap can form by patches being pulled together by action of the cell's cytoskeleton, in the case of some molecules, disruption of the cytoskeleton does not prevent cap formation. Diffusion of large aggregates on a cell surface is slow, and thus we propose that a cap can form solely through the diffusion of small aggregates containing just one or a few cell surface molecules. Here we consider the extreme case in which single molecules are mobile, but aggregates of all larger sizes are immobile. We show that a set of patches in equilibrium with a "sea" of free cell surface molecules can undergo a nucleation type phase transition in which the largest patch will bind free cell surface molecules, deplete the concentration of such molecules in the "sea", and thus cause the other patches to shrink in size. We therefore show that a cap can form without patches having to move, collide with each other, and aggregate.

1 Introduction

When multivalent ligands interact with cell surface molecules, such as the immunoglobulin (Ig) receptor on the surface of a B-lymphocyte or the major histocompatibility (MHC) antigens found on the surface of all mammalian cells, a redistribution of the cell surface molecules may take place. At 37° C the receptors first form small microscopic clusters, called *patches*. Under normal circumstances the patches coalesce, forming a single macroscopic cluster called a *cap*[1]. In the case of surface Ig, the cap is thought to form by an active, energy-requiring process involving the cell's cytoskeleton. A second mechanism may apply to the capping of MHC antigens, the Thy.1 antigen on T lymphocytes, as well as some other cell surface molecules[2,3,4,5], that is thought to depend on receptor diffusion and aggregation via ligand cross-linking.

In Figure 1, we illustrate the time dependent formation of cell surface aggregates generated by cross-linking cell surface immunoglobulin at 4° C. By 6 hours, large aggregates are observed. At 4° C, energy-dependent processes are inhibited and thus this figure illustrates the type of aggregation that we analyze below.

Figure 1 Illustration of time-dependent formation of cell surface aggregates (anti IgE-IgE-receptor complexes) at 4° C. (A) initial configuration, (B) 15 minutes, (C) 30 minutes, (D) 2 hours, (E) 4 hours, (F) 6 hours. Bar (in F) represents: (A) 0.5 μm, (B)–(F) 1 μm. The photographs show that an initially disperse set of molecules (A), when cross-linked by antibody, form extremely large aggegates (F). Micrographs were provided by Dr. J. M. Oliver and Ms. J. R. Pfeiffer, Department of Pathology, University of New Mexico Health Sciences Center.

In this paper we propose a novel mechanism for the formation of a cap that involves neither the active pulling together of small patches by the cytoskeleton nor the crosslinking of patches brought together by diffusion. The mechanism we propose is one of nucleation and growth. Basically, the idea is as follows: the normal process of patching builds up a set of microaggregates on the cell surface. The patches are of a range of sizes, some small, some large. Patches are thought to interact more strongly with the cytoskeleton than single receptors do and to diffuse much more slowly. In fact, in the case of cell surface bound immunoglobulin E aggregates larger than dimers rapidly become immobilized[6]. Thus, if patches diffuse more slowly or not at all as they become larger, it is not likely that they will coalesce into a cap by passive means. However, by comparison free receptors diffuse rather rapidly.

If a large patch has free reactive sites then it can interact with a free receptor. The addition of a receptor to the patch causes it to grow and lowers the concentration of free receptors. If larger patches have more growth sites than small patches, they will capture more free receptors than small patches and grow even bigger, allowing them to capture an ever increasing fraction of the remaining receptors. Because receptor-ligand interactions are reversible, the depletion of the free receptor concentration below its equilibrium value must cause a dissociation of receptors from the ends of existing patches of all sizes. If larger patches have proportionally fewer sites at which receptors can dissociate than smaller patches, this can result in a size-dependent balance between association and dissociation rates which is key to our theory. Thus, as large patches preferentially grow, small patches must keep supplying single receptors to the mobile pool. The net effect is that small patches disappear, and the largest patch grows into a cap. Interestingly, in this mechanism only single receptors need be transported along the surface so that the slow down in diffusion with increases in the patch size do not limit the rate of formation of the cap.

Our theory is very closely related to classical nucleation theory in which a droplet that reaches a critical radius continues to grow whereas droplets that do not reach critical size disappear. The attainment of critical size, at which surface and volume energies balance, is called nucleation. The analogous size dependent balance for a patch may be found in the ratio of growth sites versus breakable bonds. Naturally, the critical size depends on the amount of supersaturation in the medium. As larger nuclei keep depleting the medium by their growth, the instantaneous critical radius keeps increasing.

Below we develop a detailed chemical model for the polymerization of trivalent monomers which exhibits the properties required of a nucleation theory: aggregates over some critical size grow whereas small aggregates shrink. The use of trivalent monomers is a convenient approximation which demonstrates our thesis. In capping, at least two separate classes of molecules must interact, multivalent antigen and cell surface molecules. If the cell surface molecules are bivalent, they act as bridges between the ligands, and to some extent the topology of the resulting aggregate reflects the ligand's valence. In a more refined theory, one can incorporate both ligands and receptors, but existing theory indicates that the polycondensation of trivalent monomers captures all the major effects that are also seen in the receptor-ligand system[7,8].

2 The Model

We assume that trivalent monomers self associate by any of the three sites on one monomer reversibly reacting with a free site on any other monomer or aggregate of monomers. Intramolecular rearrangements of aggregates are ignored, and thus the aggregate will resemble a tree. In the

initial stage of the process during which patches form, monomers are plentiful and hence many small nearby aggregates form. Because aggregates are close together, diffusion does not provide a substantial impediment to aggregate growth, and any two aggregates can react with one another to form a larger aggregate as in classical polycondensation reactions. As the aggregates grow larger, there necessarily will be fewer aggregates on the cell surface and diffusion will become increasingly important in bringing aggregates together. Here we focus on this second stage of the process. To model it, we take an extreme point of view and assume that aggregates containing two or more monomers do not diffuse at all, whereas monomers diffuse freely. Under this assumption, only monomers move and hence only addition reactions can occur. As is usual in nucleation studies, we shall proceed by ignoring spatial variation in the various concentrations. We shall thus derive expressions for the (spatially homogeneous) concentrations of polymers of different sizes growing by depletion of the monomer background. Related models in which monomers move and aggregates are stationary have been employed to study sequential adsorption on lattices[9].

The random polycondensation of trivalent monomers has been studied beginning with Flory[10,11], Stockmayer[12] and most recently, in the context of cell surface reactions, by Perelson and Goldstein[8] and Macken and Perelson[14]. For this problem, the equilibrium distribution of aggregate sizes is known as a function of the total monomer concentration and the three equilibrium constants characterizing the binding of a monomer to a free site on another monomer containing three free sites, on a polymer unit containing two free sites, and on a polymer unit containing one free site, respectively[8]. The kinetics of polycondensation reactions have also been described for both solution phase and cell surface reactions[12,13,14,15].

The addition reactions of the type needed by our theory have not been as well studied and will be the focus of our attention. Only a subclass of dissociation reactions lead to monomer release. In order to keep track of these, we characterize an aggregate by two parameters: n, the number of monomers in the aggregate and m, the number of "ends". By an end, we mean a monomer attached to the polymer by a single bond. Thus an end has two free reactive sites. The number of ends in a tree is simply the number of branch points $+2$. Thus, an equivalent characterization could use nodes and branch points[8].

Polymers can be represented by graphs (Figure 2). In the standard notations of graph theory, each monomer corresponds to a node in the graph. The degree of a node is the number of line segments or "branches" that intersect it. Thus, an "end" is a node of degree 1. A node of degree 2 corresponds to a polymer subunit containing one free reactive site and which acts as a connector in the graph. A node of degree 3 is fully connected (i.e., has no free reactive sites). As a shorthand, we shall sometimes refer to a node of degree i as an i-node, and to 2-nodes and 3-nodes as "internal" nodes. Also, we will call an end attached to an i-node an "i-end". Again, see Figure 2. We define $C_{n,m}(t)$ to be the concentration of a polymer with n nodes and m ends at time t. In what follows, we shall refer to these aggregates as "(n,m)-trees". Various quantities associated with an (n,m)-tree, constructed from monomers of valence f, are given in Table 1 (left), and quantities specific to an (n,m)-tree constructed from monomers of valence 3 are presented in Table 1 (right).

We discuss now the combinatorics associated with reversible monomer addition reactions. We restrict our consideration to the case of trivalent monomers, i.e., $f = 3$. The chemical reactions are governed by the following rate constants:

$k_m^{\pm}$: association (dissociation) rate constant of monomer with monomer (initiation)

$k_s^{\pm}$: association (dissociation) rate constant for monomer adding to an end site (stretching/shrinking)

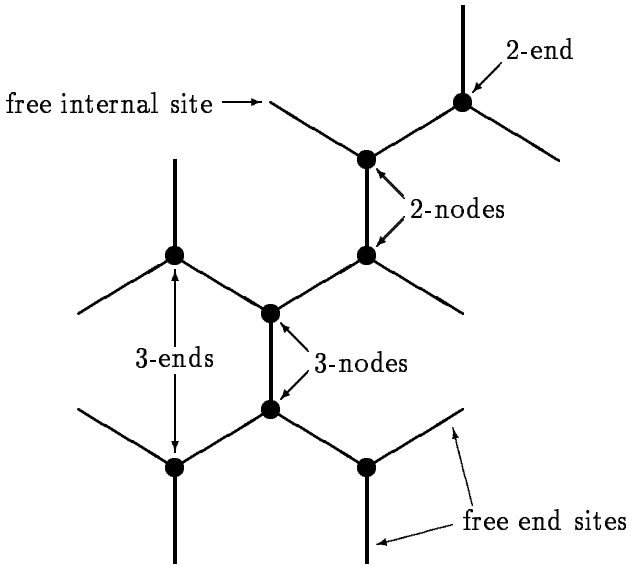

Figure 2 Schematic representation of a tree consisting of 8 nodes and 4 ends [an (8,4)-tree], showing naming conventions for nodes, ends and free sites. Angles are fictitious.

Total sites	fn
Occupied sites	$2(n-1)$
Free sites	$(f-2)n+2$
Free end sites	$(f-1)m$
Free internal sites	$(f-1)(n-m)-n+2$

Total sites	$3n$
Occupied sites	$2(n-1)$
Free sites	$n+2$
Free end sites	$2m$
Free internal sites	$n-2m+2$
Ends (1-nodes)	$2 \leq m \leq \lfloor n/2 \rfloor + 1$
2-nodes	$n-2m+2$
3-nodes	$m-2$

Table 1 Properties of an (n,m)-tree with (left) arbitrary valence f, (right) $f=3$. $\lfloor n/2 \rfloor$ is the greatest integer less than or equal to $n/2$.

Total sites	$3(n-m)$
Sites that were occupied by ends	m
Sites occupied by kernel bonds	$2(n-m-1)$
Previously existing free sites	$n-2m+2$
(belonging to 2-nodes of the original tree)	
Sites available to ends	$n-2$ $[=2$(3-nodes) + (2-nodes)$]$

Table 2 Properties of the kernel of an (n,m)-tree, $f=3$.

$k_b^{\pm}$: association (dissociation) rate constant for monomer adding to an internal site (branching/breaking)

An (n,m)-tree can grow by binding a monomer at any of its $n+2$ free sites, while it can decay by dissociation of any of its m ends. Growing, it can become an $(n+1,m)$-tree by attachment of a monomer to an end site. This "stretches" an existing branch and occurs at a rate k_s^+. The tree can also become an $(n+1,m+1)$-tree by attachment of a monomer to an internal site, generating a new branch ("branching") and this will occur at a rate k_b^+. Decaying, it can become either an $(n-1,m)$-tree or an $(n-1,m-1)$-tree according to whether the end lost was a 2-end ("shrinking" an existing branch, rate k_s^-) or a 3-end ("breaking off" an existing branch, rate k_b^-). Since the numbers of 3-nodes involved differ, the rates for stretching and branching will generally be different. The problem of enumerating the number of ways that each process can occur for a tree of a given size is not fully determinable within this level of characterization of trees, in which only their size and number of ends is recorded. As we shall show in subsequent sections, a more complete description is not needed when the rates of stretching and branching are not too different. This may be the case in many biological situations. Further, as a first model, this level of description has advantages since we are able to incorporate all the fundamental chemical processes into the model while requiring a minimal set of assumptions.

To proceed, we make a "scaling" assumption that allows us to estimate the relative probabilities of branching and stretching. We define the "kernel" of an (n,m)-tree to be the tree of $n-m$ nodes formed by removing the m ends from the original tree. Its properties are given in Table 2. Although $2(n-m-1)$ sites must be occupied by kernel-kernel bonds and m by kernel-end bonds (Table 2), the distribution of these two types of bonds among 2- and 3-nodes varies among different tree configurations. Clearly, each kernel node will have at least one site used for connecting to another node in the kernel. This leaves $n-2m+2$ sites on 2-nodes and $2(m-2)$ sites on 3-nodes of the original tree whose disposition might be different from one configuration to another, and to which either an end or a kernel node might attach. We shall assume that all possibilities can occur with equal probability. Thus, we assign a probability of $p_2(n,m) \equiv (n-2m+2)/(n-2)$ to an end being attached to a 2-node and $p_3(n,m) \equiv 1-p_2(n,m) = 2(m-2)/(n-2)$ to it being attached to a 3-node. By making this assumption and incorporating it into our kinetic scheme for addition reactions (see below), we have ignored the possibility of producing a distribution of tree shapes that leads to fractions of ends attached to 2-nodes and 3-nodes significantly different from the above computed averages. This assumption is examined below by Monte Carlo methods.

3 Analysis of the Polymerization Reactions

We formulate the problem of aggregation of trivalent monomers by addition reactions as a set of polymerization reactions. Defining $C_1(t)$ to be the instantaneous concentration of monomer, the law of mass-action leads to the following rate equations for the concentrations $C_{n,m}$. The range of allowed n and m values is depicted in Figure 3.

$$\begin{aligned}
\frac{dC_{n,m}}{dt} &= 3k_s^+(2m)C_1C_{n-1,m} + 3k_b^+(n-2m+3)C_1C_{n-1,m-1} \\
&\quad -3k_s^+(2m)C_1C_{n,m} - 3k_b^+(n-2m+2)C_1C_{n,m} \\
&\quad -k_s^-\left(\frac{n-2m+2}{n-2}\right)mC_{n,m} - k_b^-\left(\frac{2m-4}{n-2}\right)mC_{n,m} \\
&\quad +k_s^-\left(\frac{n-2m+3}{n-1}\right)mC_{n+1,m} + k_b^-\left(\frac{2m-2}{n-1}\right)(m+1)C_{n+1,m+1} \\
&\quad (n \geq 5,\ 3 \leq m \leq \lfloor (n+1)/2 \rfloor) \\
\frac{dC_1}{dt} &= -9k_m^+C_1^2 - 3k_s^+C_1\sum_{n,m=2}^{\infty}(2m)C_{n,m} - 3k_b^+C_1\sum_{n,m=2}^{\infty}(n-2m+2)C_{n,m} \\
&\quad +2k_m^-C_{2,2} + k_s^-\sum_{n,m=2}^{\infty}\left(\frac{n-2m+2}{n-2}\right)mC_{n,m} + k_b^-\sum_{n,m=2}^{\infty}\left(\frac{2m-4}{n-2}\right)mC_{n,m} \\
\frac{dC_{2,2}}{dt} &= \frac{9}{2}k_m^+C_1^2 - 12k_s^+C_1C_{2,2} - k_m^-C_{2,2} + 2k_s^-C_{3,2} \\
\\
\frac{dC_{n,2}}{dt} &= 12k_s^+C_1C_{n-1,2} - 12k_s^+C_1C_{n,2} - 3k_b^+(n-2)C_1C_{n,2} - 2k_s^-C_{n,2} + 2k_s^-C_{n+1,2} \\
&\quad +k_b^-\left(\frac{6}{n-1}\right)C_{n+1,3} \qquad (n \geq 3) \\
\frac{dC_{2n,n+1}}{dt} &= 3k_b^+C_1C_{2n-1,n} - 6k_s^+(n+1)C_1C_{2n,n+1} - k_b^-(n+1)C_{2n,n+1} \\
&\quad +k_s^-\left(\frac{n+1}{2n-1}\right)C_{2n+1,n+1} \qquad (n \geq 2)
\end{aligned}$$

We first study the possible equilibrium solutions of the above system. Setting all time derivatives equal to zero, we use the fact (detailed balance) that each reaction between two states is in equilibrium. The balance equations for reactions into and out of a general polymer state give

$$\begin{aligned}
6k_s^+C_1C_{n-1,m} &= k_s^-\left(\frac{n-2m+2}{n-2}\right)C_{n,m} \\
3(n-2m+3)k_b^+C_1C_{n-1,m-1} &= 2k_b^-\left(\frac{m-2}{n-2}\right)mC_{n,m} \\
\frac{9}{2}k_m^+C_1^2 &= k_m^-C_{2,2}
\end{aligned}$$

and two more redundant equalities. The detailed balance relations for the monomer rate equation follow by summing the above equations and are also omitted as redundant. Figure 3 shows the relationship between polymers of different sizes and illustrates how all equilibrium concentrations can be deduced once the equilibrium concentration of the monomer is known. A state is related to the one directly to the left and below it (i.e., $C_{n,m}$ is related to $C_{n-1,m-1}$) until the state with two

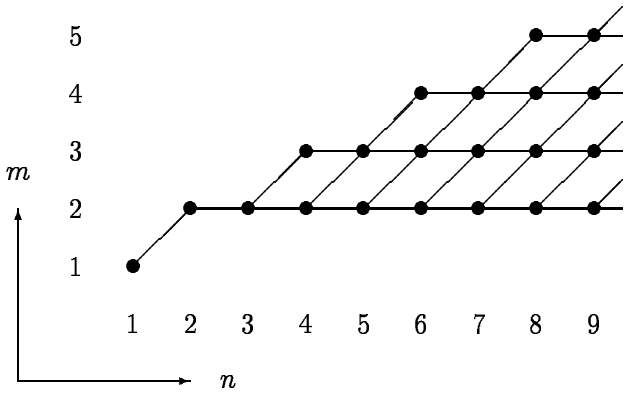

Figure 3 Tree state diagram for monomer addition and deletion.

ends is reached, which is then expressed in terms of the one below it, etc. Thus, we arrive at the following expressions, giving $C_{n,m}$ in terms of C_1 and the reaction rates:

$$\begin{aligned} C_{2,2} &= \frac{9}{2} K_m C_1^2 \\ C_{n,2} &= (6K_s C_1)^{n-2} C_{2,2} \\ C_{n+\ell,2+\ell} &= \binom{n+\ell-2}{\ell} \binom{n-2}{\ell} \frac{(3K_b C_1)^\ell}{(\ell+2)(\ell+1)2^{\ell-1}} C_{n,2} \\ & \quad (0 \le \ell \le n-2), \end{aligned}$$

where we have introduced the equilibrium constants

$$K_m := \frac{k_m^+}{k_m^-}, \quad K_s := \frac{k_s^+}{k_s^-}, \quad K_b := \frac{k_b^+}{k_b^-} \,. \tag{1}$$

(Throughout, the notation := and =: are used for definitions.) Using these recursion relations, one can show for $n \ge 2$, $m \ge 2$

$$C_{n,m} = \binom{n-2}{m-2} \binom{n-m}{m-2} \frac{4K_m}{m(m-1)K_b^2} (6K_s C_1)^n \left(\frac{K_b}{4K_s}\right)^m$$

or

$$C_{n,m} = \frac{(n-2)!}{(n-2m+2)!\, m!\, (m-2)!} \frac{4K_m}{K_b^2} \alpha^n r^m \,, \tag{2}$$

where

$$\alpha := 6K_s C_1 \quad \text{and} \quad r := \frac{K_b}{4K_s} \,. \tag{3}$$

To determine C_1, the equilibrium concentration of free monomer, we impose the condition of total mass conservation. We have, with C_0 the total concentration of monomer in all configurations,

$$C_0 = C_1 + \sum_{n=2}^{\infty} \sum_{m=2}^{\lfloor \frac{n}{2} \rfloor + 1} n C_{n,m}$$

or equivalently,

$$\alpha_0 = \alpha + \rho \sum_{n=2}^{\infty} \sum_{m=2}^{\lfloor \frac{n}{2} \rfloor + 1} n c_{n,m} =: \alpha + \rho G_\infty(\alpha, r) \tag{4}$$

where we have defined

$$\alpha_0 := 6 K_s C_0, \quad \rho := \frac{24 K_m K_s}{K_b^2}, \quad c_{n,m} := \frac{(n-2)!}{(n-2m+2)!\, m!\, (m-2)!} \alpha^n r^m, \tag{5}$$

and

$$G_\infty(\alpha, r) := \sum_{n=2}^{\infty} \sum_{m=2}^{\lfloor \frac{n}{2} \rfloor + 1} n c_{n,m}(\alpha, r). \tag{6}$$

The subscript on $G_\infty(\alpha, r)$ indicates that we have assumed the system is infinite in size, so that arbitrarily large aggregates can grow. Later, we shall examine the effect of limiting aggregates to a finite size. The nondimensional total monomer concentration α_0 will be an important parameter in what follows.

Solving (4) for α determines C_1 via (3) and completes the equilibrium description of the aggregate size distribution. An equivalent equilibrium description has been derived by Perelson and Goldstein[8] who considered the aggregration of trivalent monomers by polycondensation reactions. Since both polycondensation and addition reactions may occur, and the equilibrium state is independent of the path used to derive it, both this formulation and the Perelson and Goldstein one give identical results. By a simple change of variables, (4–5) reduces to a sum analyzed by Perelson and Goldstein, resulting in the expression

$$G_\infty(\alpha, r) = \frac{-\alpha r}{2} + \frac{(1-\alpha)^2(\alpha+2) - [4\alpha^2 r + (1-\alpha)(\alpha+2)]\sqrt{(1-\alpha)^2 - 4\alpha^2 r}}{12\alpha^2} \tag{7}$$

for the scaled polymer concentration in (4), with

$$0 \le \alpha \le \frac{1}{2\sqrt{r}+1} =: \alpha_{\max} .$$

Although this formula was derived for $\alpha < \alpha_{\max}$, it remains valid for α equal to this value.

3.1 The appearance of infinite-sized aggregates (cell surface caps)

The biological problem that our model is aimed at addressing is the formation of one large aggregate on the surface of a cell, a "cap". Here, and in subsequent sections, we examine the conditions under which the formation of a cap is predicted by our model.

We start by showing that there exists a critical concentration, $C_{0,\text{critical}}$, such that if $C_0 > C_{0,\text{critical}}$, then there is no solution to the conservation equation (4). Although the sum on the right hand side of (4) goes from 0 to ∞, it does not include the point at infinity. (Such sums are defined by first considering a finite sum, say for n going from 0 to N, and then taking the limit as $N \to \infty$.) Hence, if any mass is in an infinite-sized aggregate, the conservation equation is not satisfied because the right hand side of the equation is less than the total mass. This break down in conservation of mass is a charcteristic of sol-gel phase transitions, and the amount of mass "missing" is used to determine the mass of the gel[16]. Here we show that such a transition occurs

by finding an upper bound for the right hand side of (4). Hence, for values of α_0 greater than this bound, mass must be contained in an infinite-sized aggregate. As has been done previously[13], we associate the existence of this infinite-sized aggregate with the formation of a cap.

It is clear that G_∞ is maximized for α as large as possible, hence,

$$G_{\max} := G_\infty(\alpha_{\max}, r) = \frac{r(8\sqrt{r}+3)}{6(2\sqrt{r}+1)} \,. \tag{8}$$

Accordingly, the maximum total (scaled) monomer concentration for which there will be an equilibrium solution is

$$\alpha_{0,\text{critical}} := \frac{1}{2\sqrt{r}+1} + \rho\frac{r(8\sqrt{r}+3)}{6(2\sqrt{r}+1)} = \frac{6+\rho r(8\sqrt{r}+3)}{6(2\sqrt{r}+1)} \,. \tag{9}$$

For example, if we take $K_m = K_s = K_b$, then $r = \frac{1}{4}$, $\rho = 24$, and therefore

$$\alpha_{0,\text{critical}} = 4 \quad \text{and} \quad C_{0,\text{critical}} := \frac{\alpha_{0,\text{critical}}}{6K_s} = \frac{2}{3K_s} \,. \tag{10}$$

If the total initial monomer concentration exceeds this value, the total mass in trees of finite size cannot account for the total monomer mass present, and an infinite-sized agreggate will form. As we shall discuss in Section 5, if the series (4) is truncated at finite N, which is suitable for simulations involving finite total mass, then for $\alpha \geq \alpha_{\max}$, all mass will be concentrated in the largest allowable tree with overwhelming probability.

3.2 The most probable tree of a given size

If we consider the behavior of $c_{n,m}$ for fixed n at equilibrium, we can compute a most probable shape for a tree of a given size. We do this by showing that $c_{n,m}$ has an internal maximum (i.e., for $3 \leq m \leq \lfloor n/2 \rfloor$). Suppose n is fixed and $c_{n,m}$ is a maximum. From $c_{n,m-1} \leq c_{nm} \geq c_{n,m+1}$, we find after cancellation that

$$\frac{1}{r} \leq \frac{(n-2m+3)(n-2m+4)}{m(m-2)} \geq \frac{(n-2m+1)\cdots(n-2m+4)r}{m(m+1)(m-2)(m-1)}$$

which implies that

$$\frac{m(m-2)}{(n-2m+3)(n-2m+4)} \leq r \leq \frac{(m+1)(m-1)}{(n-2m+1)(n-2m+2)} \,.$$

For large $n, m = \mathcal{O}(n)$, the above inequalities become approximate equalities and the most probable tree of size n is found to have a ratio of nodes to ends of

$$\frac{m}{n} = \frac{\sqrt{r}}{2\sqrt{r}+1} + \mathcal{O}\left(\frac{1}{\sqrt{n}}\right) \approx \frac{\sqrt{r}}{2\sqrt{r}+1} =: \lambda \,. \tag{11}$$

Note that the value of λ can vary from 0 ($K_b \ll K_s$) to $\frac{1}{4}$ ($K_b = K_s$) to $\frac{1}{2}$ ($K_b \gg K_s$). Equation (11) implies that the geometrical properties of the most likely tree for a given n depend only on r, and not on α or α_0.

description	antigen	chemical model	physical units
association rate constants	$\bar{k}^+$	$\frac{k^+}{N_A V_{\text{reaction}}}$	sec^{-1}
dissociation rate constants	$\bar{k}^-$	k^-	sec^{-1}
equilibrium constants	$\bar{K}$	$\frac{K}{N_A V_{\text{reaction}}}$	—
initial number of monomers	N	$N_A V_{\text{reaction}} C$	—
scaled monomer equilibrium conc.	$\alpha = 6\bar{K}_s N$	$\alpha = 6K_s C$	—
simulated time	$\bar{t}$	t	sec

Table 3 Relationships between parameters corresponding to the antigen program and those defined in the chemical model. Here, the three forward reaction rate constants $\bar{k}_m^+$, $\bar{k}_s^+$, $\bar{k}_b^+$ are abbreviated by $\bar{k}^+$, and correspondingly for the reverse rate and equilibrium constants. The physical units of the parameters used by antigen are given in the rightmost column, where — denotes a dimensionless quantity.

4 Monte Carlo Simulations

We simulated the kinetics of monomer association/dissociation using a computer program, antigen. antigen starts with an initial finite pool of monomers and performs a single association/dissociation event per timestep. The progress of a particular simulation is determined by the initial size of the monomer pool (N), the reaction rate constants $\bar{k}_m^\pm$, $\bar{k}_s^\pm$ and $\bar{k}_b^\pm$, and the seed for the pseudo-random number generator. The reaction rate constants $\bar{k}^\pm$ used in antigen are proportional to the chemical reaction rate constants $k^\pm$ defined in Section 3 (discussed below). Details on the algorithm used are given in Appendix A. A typical calculation, run for one million steps, starting with an initial pool of 1000 monomers, takes a few minutes of CPU time on a Sun SPARC 10. All results reported are ensemble averages taken over 100 distinct runs, except for the 2000 node simulations which are averaged over 25.

4.1 Physical Considerations and Parameters

For antigen-antibody reactions in solution, typical reaction rate constants are $k^+ = 10^5\,(\text{M sec})^{-1}$ and $k^- = 0.01\text{–}1\,\text{sec}^{-1}$, where M := moles/liter[17]. For simplicity, we set $k_m^+ = k_b^+ = k_s^+$ and $k_m^- = k_b^- = k_s^-$, so that typical values of the equilibrium constants will be $K_m = K_b = K_s = 10^5\text{–}10^7\,\text{M}^{-1}$. Since the reactions that we are modeling occur on a cell surface, we can assume that the reaction volume is a layer, say 10 nm thick, around the surface of a cell which can be modeled as a sphere of radius 4 μm. Thus, the region in which the reactions occur is a spherical shell of volume $V_{\text{reaction}} = 2 \times 10^{-15}$ liter. Given the number of molecules in a mole, $N_A = 6 \times 10^{23}\,\text{mole}^{-1}$, N monomers in the reaction volume will correspond to a concentration $C_{0,N} := N/(N_A V_{\text{reaction}}) = N/(1.2 \times 10^9\ \text{M}^{-1})$.

For example, if we take $K_m = K_b = K_s$, then the critical concentration $C_{0,\text{critical}} = \frac{2}{3}/K_s$ (see equation 10). In the simulations, which use monomer number, the critical number of monomers $N_{\text{critical}} := \frac{2}{3} N_A V_{\text{reaction}}/K_s$. For $V_{\text{reaction}} = 2\,\mu\text{m}^3$ and $K_s = 10^6\,\text{M}^{-1}$, this gives $N_{\text{critical}} = 800$ molecules. For test runs, if we employ $K_s = 10^7\ \text{M}^{-1}$, then $N_{\text{critical}} = 80$ molecules. In this case,

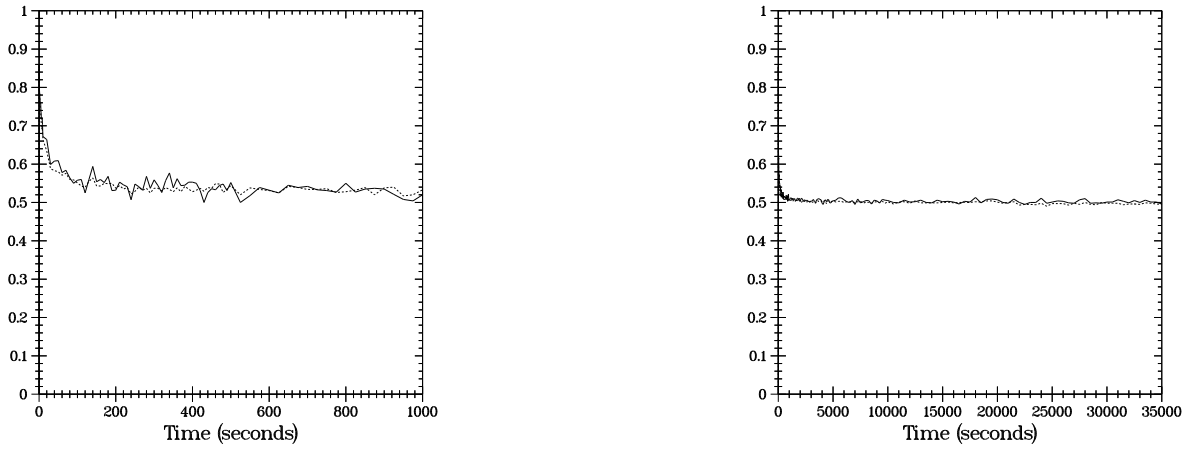

Figure 4 Computed (solid line) and predicted (dashed line) values of $p_2(n,m)$ versus time for $\bar{k}^+ = \bar{k}^- = 1$ and (a) $N = 50$, (b) $N = 2000$.

the relative probability for a binary disassociation will be of order 10^{-2}. In the analysis, we scale concentrations with K_s, so we will employ the same scaling for the simulations. The relationships between antigen parameters and the chemical parameters are given in Table 3.

4.2 Computations

To validate our statistical assumption about the relative probability of 2-ends and 3-ends (see Section 2), we examined the relative probability of an end being attached to a 2-node, $p_2(n,m)$, comparing the theoretical value, $(n-2m+2)/(n-2)$, to that obtained by simulation. Comparing Figure 4a generated with $N = 50$ to Figure 4b generated with $N = 2000$, for the case $\bar{K}_m = \bar{K}_s = \bar{K}_b = \bar{K} = 1$, one sees that in both cases, the theoretical curve approaches the Monte Carlo results, although fewer nodes imply stronger statistical fluctuations. A cell typically contains 5×10^4 to 10^5 MHC molecules, so we expect excellent agreement for this number of nodes. For the situation in which the equilibrium constants are not all equal, the agreement with theory was also extremely good. In general, if $\bar{K}_s \gg \bar{K}_b$, then long, skinny trees are produced and $p_2 \approx 1$. If $\bar{K}_b \gg \bar{K}_s$, then full, branched trees are created and $p_2 \approx 0$. (If $\bar{K}_m \gg \bar{K}_s$ and $\bar{K}_b$, then numerous little trees are formed.)

Using the results of Table 1, the ratio of free internal sites to free end sites in an (n,m)-tree of valence f is given by

$$\mu := \frac{(f-1)(n-m)-n+2}{(f-1)m} = \left(\frac{f-2}{f-1}\right)\frac{n}{m} - 1 + \frac{2}{(f-1)m}\,.$$

If n is sufficiently large and $K_b > 0$, then m on average will also be large. Using equation (11), μ can then be written

$$\mu \approx \left(\frac{f-2}{f-1}\right)\frac{1}{\lambda} - 1\,, \quad \text{and hence,} \quad \frac{n}{m} \approx \frac{1}{\lambda} \approx \left(\frac{f-1}{f-2}\right)(\mu+1)\,. \tag{12}$$

For $f = 3$, $\frac{n}{m} \approx 2(\mu+1)$.

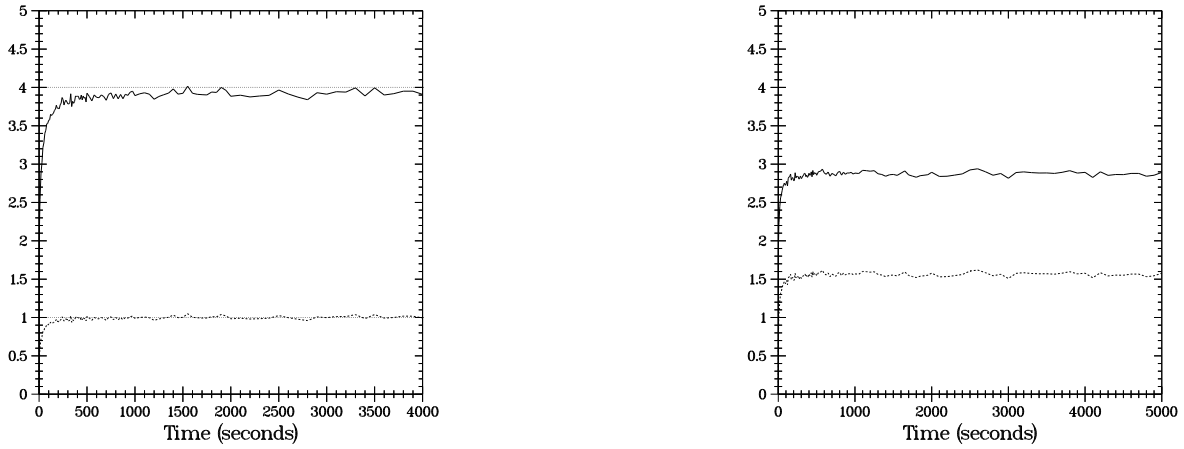

Figure 5 $\frac{n}{m}$ (solid line) and μ (dashed line) versus time for $\bar{k}^+ = \bar{k}^- = \bar{K} = 1, N = 100$ and (a) $f = 3$, (b) $f = 10$.

	$\alpha_0 = 6\bar{K}_s N$				μ			
$\bar{K}_m = \bar{K}_s = \bar{K}_b$	$N = 50$	100	200	500	$N = 50$	100	200	500
0.001	0.3	0.6	1.2	3.0	0.101	0.185	0.331	0.608
0.01	3.0	6.0	12.0	30.0	0.577	0.780	0.901	0.964
0.1	30.0	60.0	120.0	300.0	0.931	0.977	0.981	0.992

	number of trees				$n_{\max}/N$			
$\bar{K}_m = \bar{K}_s = \bar{K}_b$	$N = 50$	100	200	500	$N = 50$	100	200	500
0.001	6.688	18.714	41.620	80.025	0.072	0.053	0.050	0.090
0.01	8.636	10.400	10.263	9.689	0.285	0.424	0.643	0.860
0.1	2.152	2.039	1.961	1.905	0.840	0.919	0.961	0.982

Table 4 Asymptotic values averaged over 100 runs.

Figure 5a shows that after an initial transient, μ is effectively 1 and $\frac{n}{m}$ is just below 4 as predicted above. Here $N = 100$ and $\bar{K}_m = \bar{K}_s = \bar{K}_b = 1$ (higher equal equilibrium values produced nearly identical results). Varying the number of nodes and equilibrium constants, the behavior of μ and $\frac{n}{m}$ follows the same trends as the relationship between the actual and theoretical $\frac{2-\text{ends}}{3-\text{ends}}$ did in Figure 4. Moreover, equation (12) tracks $\frac{n}{m}$ well for valences other than 3, as shown in Figure 5b for $f = 10$, where we expect $\frac{n}{m} \approx \frac{9}{8}(\mu + 1)$.

The theory presented in Section 3 suggests that a sol-gel like phase transition should occur as α_0 passes a critical value. In Figure 6, we show the total number of trees and the size of the largest tree, $n_{\max}$, as a function of time. The results are for N taking on values from 50 to 500 and $\bar{K}_m = \bar{K}_s = \bar{K}_b$ ranging from 0.001 to 0.1, which correspond to the range $\alpha_0 = 0.3$ to $\alpha_0 = 300$ (see Table 4). For equal values of the equilibrium constants, the critical value $\alpha_{0,\text{critical}} = 4$. The panels of this figure span a transition from a number of uncoalesced, smaller trees ($\alpha_0 < \alpha_{0,\text{critical}}$) to one large "cap-like" tree that consists of essentially all the nodes available ($\alpha_0 > \alpha_{0,\text{critical}}$).

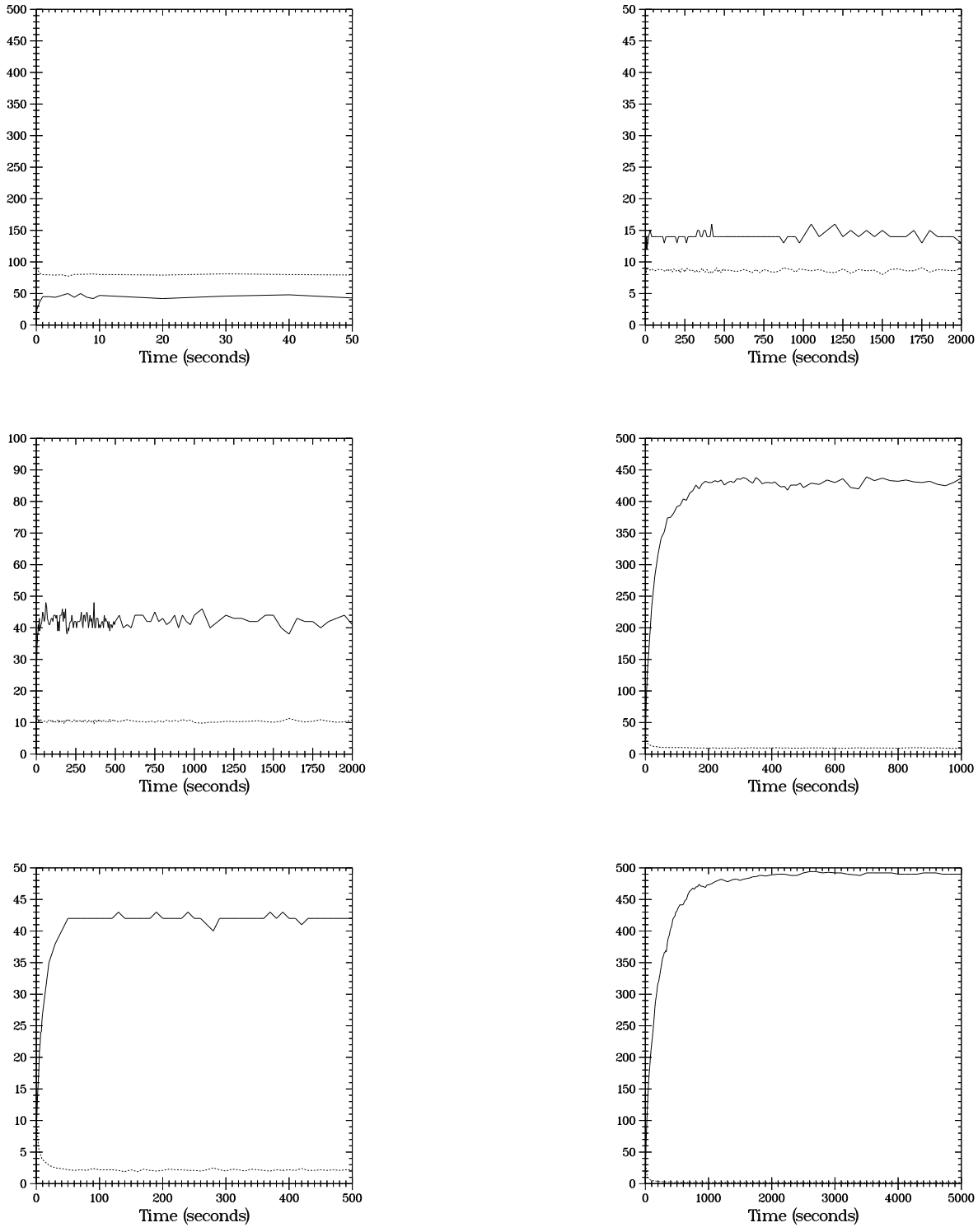

Figure 6 $n_{\max}$ (solid line) and the number of trees (dashed line) versus time for (a) $\bar{K} = 0.001, N = 500, \alpha_0 = 3$, (b) $\bar{K} = 0.01, N = 50, \alpha_0 = 3$, (c) $\bar{K} = 0.01, N = 100, \alpha_0 = 6$, (d) $\bar{K} = 0.01, N = 500, \alpha_0 = 30$, (e) $\bar{K} = 0.1, N = 50, \alpha_0 = 30$, (f) $\bar{K} = 0.1, N = 500, \alpha_0 = 300$. $\bar{k}^+ = 1$ for all cases.

$\bar{K}_m = \bar{K}_s = \bar{K}_b$	$\tilde{\tau}$
10^{-2}	69267.9 ± 6839.7
10^{-1}	750.448 ± 43.336
10^{0}	432.928 ± 25.065
10^{1}	446.103 ± 24.769
10^{2}	431.445 ± 24.905
10^{3}	454.905 ± 26.782
10^{4}	447.663 ± 26.062

N	$\tilde{\tau}$
50	166.4 ± 11.7
100	447.7 ± 26.1
200	1073.0 ± 61.8
500	3197.1 ± 178.4
1000	7233.1 ± 442.1
2000	18965.2 ± 2502.1

f	$\tilde{\tau}$
2	1552.98 ± 91.86
3	447.66 ± 26.06
4	331.29 ± 17.64
5	327.12 ± 19.87
10	293.44 ± 15.29

Table 5 The mean and standard deviation of $\tilde{\tau}$ averaged over 100 runs. (left) $f = 3$ and $N = 100$, (center) $f = 3$ and $\bar{K}_m = \bar{K}_s = \bar{K}_b = 10^4$, (right) $N = 100$ and $\bar{K}_m = \bar{K}_s = \bar{K}_b = 10^4$.

The asymptotic trends taken by μ, the number of trees and $n_{\max}/N$ are presented in Table 4. Below the phase transition, as N increases, so does the number of trees, with $n_{\max}/N$ remaining fairly constant. Above the phase transition, increasing N results in fewer trees and a monotonically increasing value of $n_{\max}/N$, indicating that the system is becoming dominated by a single tree. Furthermore, increasing N and/or increasing the $\bar{K}$'s results in $\mu \to 1$, $\frac{n}{m} \to 4$, so that the simulation ratio of 2-ends to 3-ends asymptotically approaches the theoretical mean-field value.

Let the time of formation of the cap-like tree be called τ and the corresponding dimensionless time of formation $\tilde{\tau} = \bar{k}_s^- \tau$. In Table 5, we show how $\tilde{\tau}$ varies with the simulation parameters. Notice that for constant N and equal equilibrium constants (Table 5 (left)), $\tilde{\tau}$ becomes independent of the value of $\bar{K}$ once $\alpha_0 = 6K_sN$ is is substantially greater than its critical value. Further, Table 5 (center) shows that for equal $\bar{K}$'s, the data fits the power law $\tilde{\tau} \approx N^{1.3}$, which allows one to extrapolate our results to numbers of nodes larger than what is easily simulated. Lastly, Table 5 (right) shows that, as one might expect, aggregation is faster if the molecules have a larger number of reactive sites. We remark that for the typical case, the time of cap formation is dominated by the monomer dissociation rate.

5 Phase Transition

In comparing the conclusions reached by the equilibrium analysis in Section 3 with those of the dynamic simulations in Section 4, we must bear in mind the different statistical assumptions underlying the two approaches. The chemical analysis of Section 3 essentially assumes a large collection of systems, in which mass is conserved on average. Thus, it is not contradictory to speak of the formation of an infinite size aggregate in a system with finite mass. On the other hand, in the Monte Carlo simulations, we produce ensemble averages in which individual members of the ensemble conserve mass in detail. Consequently, in the simulations, trees of size greater than N, the total number of monomer units, cannot exist. In the simulation, there is not an abrupt transition to the gel phase. Rather, the single tree state is attained as a gradual process, as the expectation for a single tree of maximal size approaches one.

The mass conservation condition for the simulations with maximum tree size N is

$$\alpha_0 = \alpha + \rho \sum_{n=2}^{N} \sum_{m=2}^{\lfloor \frac{n}{2} \rfloor + 1} n c_{n,m} =: \alpha + \rho G_N(\alpha, r) \, . \tag{13}$$

To compare with equation (4) where infinite size trees are allowed, we note that in either case the scaled total concentration α_0 is the experimentally specified control parameter, where for the finite system

$$\alpha_0 := 6 K_s C_{0,N} = 6 K_s \left(\frac{N}{N_A V_{\text{reaction}}} \right) \, . \tag{14}$$

In the sequel, we specify whether we are using the finite system equation (13) or the infinite system equation (4) by introducing the symbols $\alpha_{0,N}$ and $\alpha_{0,\infty}$, respectively. Unlike the infinite system mass conservation equation (4), which is only defined for $0 \leq \alpha \leq \alpha_{\max}$, the plot of $\alpha_{0,N}(\alpha)$ for various values of N (Figure 7a) shows that in the finite system, the conservation equation (13) has a solution for all values of α.

As N is increased, the signature of the phase transition is seen to be an overwhelming growth of the expectation for a single tree of maximum size. The graph of the concentration, $c_{n,m}$ versus n and m shown in Figure 7b gives a clear indication of this phenomenon as follows: if $\alpha < \alpha_{\max}$, then the concentration is a strictly decreasing function of n and m along the "spine" (or line of maximum concentration) for increasing values of n and m. However, for $\alpha > \alpha_{\max}$, the concentration starts increasing along the spine for n sufficiently large, and as the growth is exponential, it can be seen that $c_{n,m}$, the expectation of a given size tree, becomes maximal for the tree of size N, and it is overwhelmingly larger than that for smaller trees (Figure 7b).

To establish this, we rewrite $c_{n,m}$ in terms of the continuous variables x and σ by setting $n = x$ $(2 \leq x \leq \infty)$, $m = \sigma x$ $(0 \leq \sigma \leq \frac{1}{2})$, and use Stirling's formula, $n! = \sqrt{2\pi n} \left(\frac{n}{e}\right)^n \left[1 + \frac{1}{12n} + \mathcal{O}\left(\frac{1}{n^2}\right)\right]$, to obtain

$$\begin{aligned} c_{x,\sigma x} &= \frac{x! \, (\sigma x - 1) \, \sigma \, \alpha^x r^{\sigma x}}{(x-1)[(1-2\sigma)x]! \, [(1-2\sigma)x + 1][(1-2\sigma)x + 2](\sigma x)!^2} \\ &= \frac{1}{2\pi} \frac{1}{\sqrt{1-2\sigma}} \frac{\sigma x - 1}{x(x-1)[(1-2\sigma)x + 1][(1-2\sigma)x + 2]} \kappa(\sigma)^x \left[1 - \mathcal{O}\left(\frac{1}{x}\right)\right] \, , \end{aligned}$$

where

$$\kappa(\sigma) := \frac{\alpha r^\sigma}{\sigma^{2\sigma}(1-2\sigma)^{1-2\sigma}} \, .$$

Now, $c_{x,\sigma x} \sim \kappa(\sigma)^x$, and $\kappa(\sigma)$ is maximized at $\sigma = \lambda = \sqrt{r}/(2\sqrt{r}+1)$ where it has the value $\kappa(\lambda) = (2\sqrt{r}+1)\alpha$. As mentioned earlier, the tree of most likely shape will exhibit the ratio $\frac{m}{n} \approx \lambda$, and thus the spine in Figure 7b will correspond to the line $m = \lambda n$, i.e., $\sigma = \lambda$. Looking along this line for parameters such that $\kappa(\lambda) < 1$, i.e., for

$$\alpha < \frac{1}{2\sqrt{r}+1} = \frac{\lambda}{\sqrt{r}} = \alpha_{\max} \, , \tag{15}$$

we expect $c_{x,\lambda x}$ to decrease as x increases. However, if $\alpha > \alpha_{max}$ so that $\kappa(\lambda) > 1$, $c_{x,\lambda x}$ will increase exponentially as x increases and the expected size of a tree will be maximal when $x = N$.

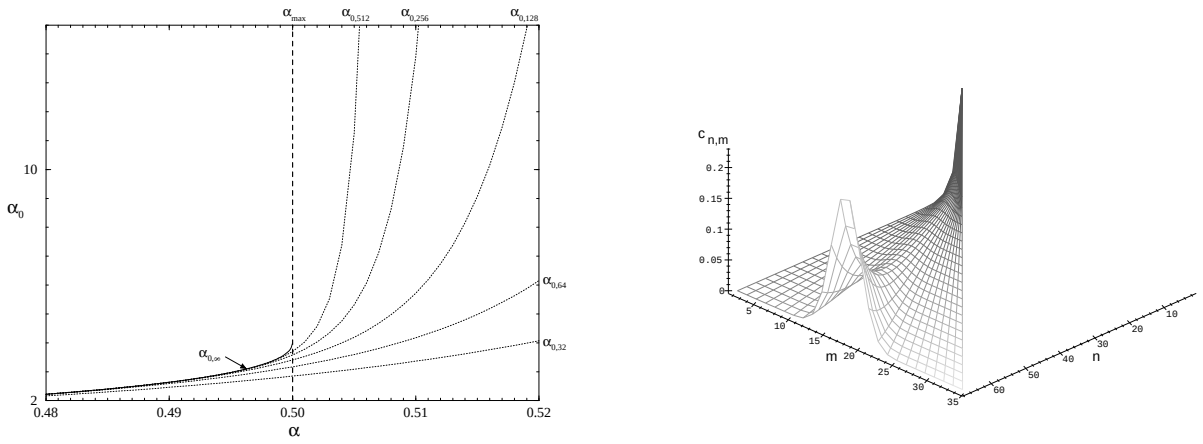

Figure 7 (a) $\alpha_{0,\infty}(\alpha)$ (solid line) and $\alpha_{0,N}(\alpha)$ for $N = 32, 64, 128, 256, 512$ (dotted lines), (b) equilibrium concentration c_{nm} versus n and m for $\alpha = 0.58 > \alpha_{\max} = \frac{1}{2}$ with $r = \frac{1}{4}$. Note the sharp maximum at $\frac{m}{n} = \sigma = \frac{1}{4}$ for fixed n, and the exponential rise of the maximum for increasing n (the "spine"). The spike on the right corresponds to free monomer ($n = 1$).

6 Conclusions

We have shown that a model of addition reactions between trivalent monomer units undergoes a phase transition above a critical value of $\alpha_0 = 6K_sC_0$, where C_0 is the total concentration of monomer units and K_s is the equilibrium constant for a reaction between a monomer and the end of an existing aggregate. This type of transition could underly the phenomenon of capping observed on the surface of many types of cells, such as lymphocytes. During capping, a molecule, such as an antibody which can cross-link two cell surface molecules, is added to the medium surrounding a cell. In our model, the addition of the antibody allows cell surface molecules to coalesce and hence increases all of the association constants (k_m^+, k_s^+ and k_b^+). During a capping experiment, one first observes the formation of small aggregates of cell surface molecules called patches, followed by the formation of a macroscopic aggregate, the cap. Because diffusion of large aggregates is very slow compared with the diffusion of single cell surface molecules (monomers), we have suggested that the cap can form by monomers dissociating from small aggregates, and ultimately reacting with the larger number of free sites available on large aggregates. Kinetically, this process should resemble a nucleation process, where an aggregate above a critical size will grow while aggregates below the critical size shrink. For a homogeneous system, we have shown that this is the case by Monte Carlo simulation in which we maintained a complete description of the time evolving aggregates. We also found general agreement with predictions of the phase transition made on the basis of a mean-field, mass-action based scheme of the aggregation process enlisting a two parameter model in which aggregate size and shape were characterized. We were able to show that at equilibrium,

an aggregate will have a most probable shape and so the dynamics of the phase transition are solely a function of the aggregate size (for a given set of reaction rates).

Acknowledgements

Portions of this work were done under the auspices of the U.S. Department of Energy. It was supported by NIH grants AI28433 and RR06555 (A.S.P.) and the Santa Fe Institute Theoretical Immunology Program through a grant from the Joseph P. and Jeanne M. Sullivan Foundation. We would also like to thank Ed Bedrick for his help with the statistical issues.

References

1. Taylor, R. B., W. P. H. Duffus, M. C. Raff and S. de Petris. 1971. Redistribution and pinocytosis of lymphocyte surface immunoglobulin molecules induced by anti-immunoglobulin antibody. *Nature New Biology* **233**:225–229.
2. Stackpole, C. W., J. B. Jacobson and M. P. Lardis. 1974. Two distinct types of capping of surface receptors on mouse lymphoid cells. *Nature* **248**:232–234.
3. Braun, J., K. Fujiwara, T. D. Pollard and E. R. Unanue. 1978a. Two distinct mechanisms for redistribution of lymphocyte surface molecules. I. Relationship to cytoplasmic macromolecules. *J. Cell Biol.* **79**:409–418.
4. Braun, J., K. Fujiwara, T. D. Pollard and E. R. Unanue. 1978b. Two distinct mechanisms for redistribution of lymphocyte surface molecules. II. Contrasting effects of local anesthetics and a calcium ionophore. *J. Cell Biol.* **79**:419–426.
5. Braun, J. and E. R. Unanue. 1980. B-lymphocyte biology studied with anti-Ig antibodies. *Immunol. Rev.* **52**:3–28.
6. Menon, A. K., D. Holowka, W. W. Webb and B. Baird (1986). Cross-linking of receptor-bound IgE to aggregates larger than dimers leads to rapid immobilization. *J. Cell Biol.* **102**:541–550.
7. Goldstein, B. and A. S. Perelson. 1984. Equilibrium theory for the clustering of bivalent cell surface receptors by trivalent ligands: With application to histamine release from basophils. *Biophysical J.* **45**:1109–1123.
8. Perelson, A. S. and B. Goldstein 1985. A new look at the equilibrium aggregate size distribution of self-associating trivalent molecules. *Macromolecules* **18**:1588–1597.
9. Evans, J. W. 1993. Random and cooperative sequential adsorption, *Rev. Mod. Phys.* **65**:1281–1329.
10. Flory, P. J. 1941a. Molecular size distribution in three dimensional polymers. I. Gelation. *J. Am. Chem. Soc.* **63**:3083–3090.
11. Flory, P. J. 1941b. Molecular size distribution in three dimensional polymers. II. Trifunctional branching units. *J. Am. Chem. Soc.* **63**:3091–3096.
12. Stockmayer, W. H. 1943. Theory of molecular size distribution and gel formation in branched polymers. *J. Chem. Phys.* **11**:45–55.
13. DeLisi, C. and A. S. Perelson. 1976. The kinetics of aggregation phenomena: I. Minimal models for patch formation on lymphocytes. *J. Theoret. Biol.* **62**:159–210.

Event	Weight	Unweighted probability
Creating a 2-tree from free nodes	$\bar{k}_m^+$	$\frac{1}{2}f^2$(free-nodes)(free-nodes $-$ 1)
Destroying a 2-tree	$\bar{k}_m^-$	2-trees
Attaching a node to an end site (stretching a branch)	$\bar{k}_s^+$	f(free-nodes)(end-sites)
Detaching a 2-end (shrinking a branch)	$\bar{k}_s^-$	2-ends
Attaching a node to an internal site (growing a branch)	$\bar{k}_b^+$	f(free-nodes)(internal-sites)
Detaching a ($\geq$3)-end (breaking off a branch)	$\bar{k}_b^-$	($\geq$3)-ends

Table 6 Likelihoods of possible events in an antigen run.

14. Macken, C. A. and A. S. Perelson. 1985. *Branching Processes Applied to Cell Surface Aggregation Phenomena.* Lecture Notes in Biomathematics, Vol. 58. Springer Verlag, New York.
15. Perelson, A. S. and C. DeLisi. 1975. A systematic and graphical method for generating the kinetic equations governing the growth of aggregates. *J. Chem. Phys.* **62**:4053–406l.
16. Flory, P. J. 1953. *Principles of Polymer Chemistry,* Cornell University Press, Ithaca, New York.
17. Pecht, I. and D. Lancet. 1977. Kinetics of antibody-hapten interactions. In *Chemical Relaxation in Molecular Biology*, Pecht, I. and Rigler, R., eds., Springer-Verlag, New York, pp. 306–338.

A Dynamics of the Monte Carlo Simulations

antigen is a computer program written in C. It represents a node as a data structure, with pointers to other similar data structures acting as molecular bonds. A null pointer indicates a free site. A tree is thus a collection of interconnected nodes, while an isolated node represents a monomer. Associated with each node and each tree are numbers detailing various quantities pertaining to that object, such as the number of free sites on a node or counts of 2-ends and 3-ends on a tree.

Initially, there are no trees and all the nodes are free monomers residing in a fixed pool. At the beginning of each timestep, a random event is selected to happen. The actual choice is made by picking a pseudo-random number from an interval which is divided into subintervals whose lengths represent the likelihoods of each alternative event. There are six possible events, the probability of each one weighted by a different reaction rate constant. These are illustrated in Table 6 for an arbitrary valence f, where ends attached to order 3 or greater nodes are treated as essentially similar since their removal always involves breaking a branch. The hyphenated quantities are instantaneous totals taken over the entire system. Once an event has been chosen, the site to attach to, the end to break off, or the 2-tree to break apart is randomly selected from all available possibilities. The pool of free nodes will grow or shrink accordingly.

In the program, an event takes place by modifying pointers. For example, attaching a free node to a tree requires that the node be removed from the pool of free nodes and then linked into the

tree by setting one of its formerly null pointers to point to the appropriate node on the tree where a free site of the proper kind exists. The free site is then set to point back to the former monomer, completing the bond. All bookkeeping totals are then updated and the algorithm repeats.

The simulations are event driven in the sense that exactly one association/disassociation event occurs during a single timestep. This fact permits a Poisson process to be used as a model for the simulations. A benefit of this is that the simulations can then be naturally embedded in time as the length of a timestep can be given a value which will be associated with the likelihood of the particular event that occurs during the timestep. In particular, we defined the timestep length to be in units of the reciprocal of the weighted probability of the event that takes place within (Table 6) for all of our antigen runs. These units can be converted into dimensionless quantities by multiplying by $\bar{k}_s^-$.